

The Prognostic Potential of Human Prostate Cancer-Associated Macrophage Subtypes as Revealed by Single-Cell Transcriptomics

Joseph C. Siefert^{1,2}, Bianca Cioni¹, Mauro J. Muraro^{3,4}, Mohammed Alshalalfa⁵, Judith Vivié^{3,4}, Henk G. van der Poel⁶, Ivo G. Schoots⁷, Elise Bekers⁸, Felix Y. Feng⁵, Lodewyk F.A. Wessels^{2,9}, Wilbert Zwart^{1,9}, and Andries M. Bergman^{1,10}



ABSTRACT

Macrophages in the tumor microenvironment are causally linked with prostate cancer development and progression, yet little is known about their composition in neoplastic human tissue. By performing single cell transcriptomic analysis of human prostate cancer resident macrophages, three distinct populations were identified in the diseased prostate. Unexpectedly, no differences were observed between macrophages isolated from the tumorous and nontumorous portions of the prostatectomy specimens. Markers associated with canonical M1 and M2 macrophage phenotypes were identifiable, however these were not the main factors defining unique subtypes. The genes selectively associated with each macrophage cluster were used to develop a gene signature which was highly associated with both recurrence-free and

metastasis-free survival. These results highlight the relevance of tissue-specific macrophage subtypes in the tumor microenvironment for prostate cancer progression and demonstrates the utility of profiling single-cell transcriptomics in human tumor samples as a strategy to design gene classifiers for patient prognostication.

Implications: The specific macrophage subtypes present in a diseased human prostate have prognostic value, suggesting that the relative proportions of these populations are related to patient outcome. Understanding the relative contributions of these subtypes will not only inform patient prognostication, but will enable personalized immunotherapeutic strategies to increase beneficial populations or reduce detrimental populations.

Introduction

Blood-derived monocytes reach the majority of the tissues in the body, both cancer affected and normal, where they become tissue-resident macrophages (1). However, not all tissue-resident macrophages arise from circulating monocytes, as resident macrophages are present during embryonic development and persist during adulthood (2, 3). Consequently, as in other tissues, the prostate is composed

of both embryonic-derived and blood-derived macrophages, where it remains unclear whether macrophages of distinct origins have distinct functions (4).

Macrophages are extremely plastic and phenotypically heterogeneous immune cells, whose diversity is largely influenced by the microenvironment in which they reside (5). Several studies showed that *in vitro* blood monocyte-derived macrophages can acquire a large spectrum of phenotypes depending on different stimuli present in the cell culture (6, 7). However, these models do not capture the dynamic nature of macrophages in their native microenvironment. Human tissue-specific characterization of tumor-associated macrophages (TAM) is limited to glioma, skin, and hepatocellular carcinoma (8–10), and there are no studies addressing prostate cancer (PCa)-specific macrophage phenotypic diversity.

The PCa tumor microenvironment (TME) is composed of various cells, including stromal, endothelial, and immune cells, with tissue-resident macrophages representing one of the most predominant immune cell populations (11, 12). Macrophages are critical mediators of tissue homeostasis and have the capacity to suppress cancer-associated processes, including tumor cell proliferation, angiogenesis, and metastasis (13). Multiple studies have shown a correlation between high infiltration of TAMs in the PCa microenvironment and poor prognosis, which suggests a role of these cells in cancer progression (14–18). Given the prognostic significance of macrophages in the TME, strategies aiming to target these cells have emerged as strong candidates for cancer treatment (19–22).

It is also thought that immune cell type rather than sheer numbers of immune cells present in the TME relates to efficacy (23). Various macrophage phenotypes have been described, including the pro-inflammatory/anti-tumor M1 state, and the anti-inflammatory/pro-tumor M2 state, both characterized by expression of specific markers (24). However, macrophage diversity is likely not a binary division, but rather a continuum of phenotypes between M1 and

¹Division of Oncogenomics, The Netherlands Cancer Institute, Amsterdam, the Netherlands. ²Division of Molecular Carcinogenesis, The Netherlands Cancer Institute, Amsterdam, the Netherlands. ³Single Cell Discoveries B.V., the Netherlands. ⁴Hubrecht Institute-KNAW and University Medical Center Utrecht, the Netherlands. ⁵Department of Radiation Oncology, UCSF Helen Diller Family Comprehensive Cancer Center, San Francisco, California. ⁶Division of Urology, The Netherlands Cancer Institute, Amsterdam, the Netherlands. ⁷Department of Radiology and Nuclear Medicine, The Netherlands Cancer Institute, Amsterdam, the Netherlands. ⁸Department of Pathology, The Netherlands Cancer Institute, Amsterdam, the Netherlands. ⁹Oncode Institute, the Netherlands. ¹⁰Division of Medical Oncology, The Netherlands Cancer Institute, Amsterdam, the Netherlands.

Note: Supplementary data for this article are available at Molecular Cancer Research Online (<http://mcr.aacrjournals.org/>).

J.C. Siefert and B. Cioni contributed equally to this article.

Corresponding Authors: Andries M. Bergman, Medical Oncology and Oncogenomics, The Netherlands Cancer Institute, Plesmanlaan 121, Amsterdam, 1066CX, the Netherlands. Phone: 31-20-512-2569; Fax: 31-20-512-2572; E-mail: a.bergman@nki.nl; Lodewyk F.A. Wessels, l.wessels@nki.nl; and Wilbert Zwart, w.zwart@nki.nl

Mol Cancer Res 2021;19:1778–91

doi: 10.1158/1541-7786.MCR-20-0740

This open access article is distributed under Creative Commons Attribution-NonCommercial-NoDerivatives License 4.0 International (CC BY-NC-ND).

©2021 The Authors; Published by the American Association for Cancer Research

M2 extremes (6, 7). However, the diversity of human macrophage populations in PCa is not yet explored and, therefore, tissue-specific markers of macrophage populations in PCa are not yet defined.

To address this, we applied single-cell mRNA sequencing on myeloid cells isolated from prostatectomy specimens. Here we describe novel phenotypes of PCa-associated macrophages and their distinct prognostic potential. Moreover, we propose new molecular markers for identification of these phenotypes in patients with localized disease. Understanding the unique macrophage populations in individual prostate tumors and their effect on outcome will not only enhance our knowledge of PCa biology and progression, but can better inform clinicians regarding a patients' prognosis and treatment options.

Materials and Methods

Patients, tumor specimens, and ethics statement

Prostate biopsies were collected from post-robotic-assisted laparoscopic prostatectomy (RALP) surgical specimen of patients with PCa who did not receive any prior therapy (Gleason score 3+4 and 3+3). Biopsies were collected from both the tumorous and the nontumorous site of the prostate, which were estimated by a presurgery multiparametric magnetic resonance imaging (mpMRI) scan of the pelvis and palpation by the surgeon of the prostatectomy specimen. An average of three 18G biopsies were taken from the areas of the prostate with a very high likelihood of containing clinically relevant PCa (tumorous site) and from areas of the prostate without suspected PCa (nontumorous site) on mpMRI. Accuracy of the mpMRI to identify tumorous and nontumorous areas of the prostate was histologically verified in H&E stained whole mount formalin fixed and paraffin embedded slides. Fresh biopsies from the tumorous site and nontumorous site of the prostatectomy specimen from four patients were processed separately for cell-surface markers CD14⁺ and/or CD11b⁺ myeloid cell isolation and submitted for single-cell RNA sequencing.

The occurrence of identified clusters of macrophage populations in prostatectomy specimen was estimated by IHC staining for cluster-specific marker genes, which were selected from the top 10 list of most differentially expressed genes between the clusters, which are not secreted and had the highest specificity for myeloid cells. Stained cores for the selected markers of the clusters, Cluster 0: SLC40A1 (antibody HPA065634; antibody 11 cores), Cluster 1: PLAC8 (antibody HPA040465; 21 cores), Cluster 2: FCN1 (antibody HPA001295; 32 cores), and the pan-macrophage marker CD68 (antibody CAB000051; 54 cores), were downloaded from the human protein atlas (www.proteinatlas.org) and visually estimated for percentage surface containing tumor and nontumor and for number of marker positive cells in both compartments. Marker positive cells were identified and quantified by specific marker staining and morphology by a pathologist specialized in uro-oncology. A score (0, 1, 2, or 3) was assigned on the basis of the number of macrophages present (0, 1–10, 11–100, >100), respectively. Density of marker positive cells in tumorous and nontumorous tissue was estimated by dividing the number of marker positive cells in a compartment by the fraction of the total core surface containing the compartment.

The use of patient data and biopsies from fresh prostatectomy specimens for research purposes at the Netherlands Cancer Institute have been executed pursuant to Dutch legislation and international standards. Prior to 25 May 2018, national legislation on data protection applied, as well as the International Guideline on Good Clinical Practice. From 25 May 2018 on, we also adhere to the GDPR. Within this framework, patients are informed and have always had the opportunity to object or actively consent to the (continued) use of

their personal data and biospecimens in research. For this study, informed consent was obtained from all patients. Hence, the procedures comply both with (inter-) national legislative and ethical standards.

Tissue dissociation and CD11b⁺ and/or CD14⁺ cells sorting

Single-cell suspension was prepared from fresh PCa biopsies by mechanical dissociation within 2 hours after surgery. Biopsies were transported from the operation room on ice and minced with a scalpel in cold PBS + 0.5% BSA. Tissue was then mechanically dissociated using a gentleMACS Dissociator (MACS Milteny Biotec) using C-tubes (MACS Milteny Biotec) for 2 minutes as described previously (25). Subsequently, the samples were filtered through a 70 µmol/L strainer (BD Falcon) and spun down for 5 minutes at 300 × g at 4°C. Cells were refiltered through a 40 µmol/L strainer (BD Falcon), spun down for 5 minutes at 300 × g at 4°C and resuspended in cold PBS + 0.5% BSA. To compare the efficacy of GentleMACS with enzymatic digestion, biopsies were chopped with scalpel and tweezers and transferred to a 15 mL Falcon tube containing 100 U/mL of Collagenase I (SCR103; Sigma Aldrich), 0.05% of DNase I (89836; Thermo Fisher Scientific) and 5U/mL of Hyaluronidase (H3506; Sigma-Aldrich) and incubated at 37°C for 2 hours. Enzymatic digestion was then stopped by adding 1:1 volume of FBS-containing RPMI medium to the cell suspension. A 70 µmol/L strainer was used to filter the cell suspension, followed by centrifugation at 1,200 rpm for 10 minutes. Supernatant was removed and cells were resuspended in RPMI medium containing 10% FBS.

Cells of the dissociated biopsies were incubated with APC-CD45, PE-CD14, PE-CD11b, and FITC-CD3 (all Ebioscience) for 20 minutes and washed before sorting using a MoFlo Astrios (Beckman Coulter) or FACSARIA IIu (BD BioSciences). As a first step, cell doublets/multiplets and dead cells were excluded using FSC height versus area. Then, CD45⁺ leukocytes were selected, whereas small CD45⁺ cells (low SSC) were discarded as possible lymphocytes. Subsequently, CD14⁺ and/or CD11b⁺ single cells lacking CD3 expression (lymphocytes) were selected. Living single CD45⁺CD3⁻CD14⁺ and/or CD11b⁺ macrophages (based on DAPI and scatter properties) were sorted into eight 384 wells plates (Bio-Rad) where cDNA synthesis was performed as described previously (26).

Single-cell sequencing with SORT-seq

Single-cell mRNA sequencing was performed according to an adapted version of the SORT-seq protocol (26), using barcoded poly-A primers described by van den Brink and colleagues (27). In short, single cells were FACS sorted into 384-well plates containing 384 different poly-A barcoded primers and Mineral oil (Sigma). After sorting, plates were snap-frozen on dry ice and stored at –80°C. Subsequently, cells were heat-lysed at 65°C followed by cDNA synthesis using the CEL-Seq2 protocol (28) using robotic liquid handling platforms Nanodrop II (GC Biotech) and Mosquito (TTP Labtech). After second strand cDNA synthesis of poly-A transcripts, the barcoded material was pooled into libraries of 384 cells and amplified using *in vitro* transcription (28). Following amplification, the rest of the CEL-seq2 protocol was followed for preparation of the amplified cDNA library, using TruSeq small RNA primers (Illumina) as previously described (26). The DNA library was paired-end sequenced on an Illumina Nextseq500, high output, 1 × 75 bp.

Single-cell sequencing data analysis

After Illumina sequencing, read 1 was assigned 26 base pairs and was used for identification of the Illumina library barcode and cell barcode. Unique molecular identifiers (UMI) tags were added to each

read. These are molecular tags used to detect and quantify unique mRNA transcripts. More specifically, mRNA libraries were generated by fragmentation and reverse transcribed to cDNA with tag-specific primers. Read 2 was assigned 60 base pairs and used to map to the reference transcriptome of Hg19. Data was demultiplexed as described previously (29).

The Seurat v3.1.4 package was used in R v3.6.1 for processing the data (30). To exclude dead, dying, or otherwise low-quality cells, cells with less than 1,000 features (genes) and cells with greater than 1% mitochondrial reads were removed from analysis. To exclude cell doublets/multiplets, cells with greater than 6000 features (genes) were removed from analysis. The data were log-normalized with a scale factor of 10,000, and the 2000 most variable features were identified using a variance stabilizing transformation. The data were scaled according to all detected genes and PC analysis was performed on the most variable genes. For linear dimensionality reduction, the number of PCs (20) was selected on the basis of combined Jackstraw analysis, examination of elbow plots, difference in variation between subsequent PCs, and cumulative percent variation explained (31). To identify clusters, a K-nearest neighbors graph was constructed from the selected PCs and clusters were identified from this using the Louvain algorithm at a resolution of 0.5 in Seurat. These were then projected with Uniform Manifold Approximation and Projection (UMAP) using uwot v0.1.5 and umap v0.2.4.1 packages in R.

A reciprocal PCA method was used for data integration (30). In this procedure, the data from each patient was normalized, variable features were selected, the data was scaled, and PC analysis was performed independently. The PCA space of each patient was then projected into each other patient to identify anchor points. The anchors represent matching cell states identified by pairwise correspondence between cells from different patients and are used to transform the datasets into a shared space. The integrated data were then scaled and PC analysis was performed as before. Clustering at various shared nearest neighbors (SNN) resolutions was evaluated and plotted with `clustree_0.4.3` (32).

Differential expression and gene set enrichment analysis (GSEA)

Differential expression analysis was performed on normalized RNA values with minimum percentage (`min.pct`) and log fold-change (`logfc`) thresholds of 0.25 to identify marker genes specific to each cluster. Of note, although upregulation of genes in a cluster relative to other clusters is generally reported, this implies that in the latter clusters those genes are relatively downregulated. Significant differentially expressed genes were defined by Bonferroni adjusted P value <0.05 . GSEA was performed using `clusterProfiler v3.12.0` with `msigdb v7.1.1` database in R (33). Hallmark gene set enrichment analysis was performed by calculating `logfc` for all genes in each cluster as compared with the other two clusters, without any thresholds for `min.pct` or `logfc`, and ranking genes based on `logfc`.

Generation and evaluation of gene signatures

Differentially expressed genes between macrophage clusters identified in the integrated dataset were used to construct prognostic signatures for biochemical relapse-free survival (RFS) of patients with PCa in a published MSKCC PCa dataset (GSE 21032) (34). This dataset, comprised of 131 primary patients with PCa with RNA expression and biochemical recurrence (BCR) as determined by serum prostate-specific antigen (PSA) levels, was used to assess biochemical RFS. RFS was defined as time from prostatectomy to BCR (rise of PSA ≥ 0.2 ng/mL on two occasions).

The gene signature (classifier) was generated employing Elastic net Cox regression using `glmnet v4.0` in R (35). The prognostic performance of the selected gene set was assessed in the MSKCC data by performing a nested 10-fold cross-validation (10FCV), with the full dataset split randomly into 10 folds with each fold stratified for the number of events and Gleason score. The Elastic net regularization parameters (α and λ) were optimized as follows. A pre-selected set of values for α were tested (0 to 1 by 0.1). For each value of α in this set, we performed 10FCV to determine the optimal value of λ . To this end, we selected the value of λ associated with the minimum, average mean-squared error (MSE) across the folds. This procedure delivered, for each value of α , the optimal value of λ and the associated MSE. We then selected the value of α that delivered the lowest MSE across all values of α in the set. HR, confidence intervals (CI), P values, and Harrel's C-index (concordance index) for the MSKCC evaluation were generated using the `coxph` function in the `survival v3.1-12` package in R (36). Survival plots were made by selecting the high (top 25%), low (bottom 25%), and intermediate (middle 50%) risk of relapse from the CV predictions, fit with event censoring and BCR-free time from MSKCC dataset using the `survfit` function in the `survival` package. ROC curves and AUC were calculated using predictions from the CV with `ROCR v1.0-7` in R (37). The final macrophage gene signature used for validation was generated by fitting the full MSKCC dataset with the optimized parameter values.

Validation of gene signatures in independent cohorts

Gene signatures were tested in three independent cohorts by first extracting the coefficients (β s) for the selected genes from the model fit, then multiplying the scaled gene expression data in the independent datasets by these coefficients. The prospective Decipher cohort contains anonymized genome-wide expression profiles from clinical use of the Decipher test in the radical prostatectomy (RP) setting, between February 2014 and August 2017, retrieved from the Decipher GRID (NCT02609269). The retrospective natural history cohort from Johns Hopkins Medical Institutions is comprised of men treated with RP, with a median follow up time of 108 months (38). The Mayo Clinic Cohort is a retrospective cohort of men treated with RP, with a median follow-up time of 156 months (39, 40). Model discriminatory capability was assessed on the basis of the AUC. Cox proportional hazards was used to estimate the HR of metastasis-free survival for patients with high signature (top25%).

Public availability of data

Limited and specific single cell RNA sequencing data of patient macrophages can be found at GSE133094. RNA expression data for Mayo (GSE46691, GSE62116), and JHMI (GSE79957) cohorts are also available.

Results

Single-cell analysis of myeloid cells isolated from PCa biopsies

To identify the macrophage populations present in diseased human prostates, fresh biopsies were collected from "tumorous" and "non-tumorous" areas of post-RP specimens. Four previously patients with untreated PCa, ages 50 to 74 years, with an initial serum PSA between 7.6 and 9.3 ng/mL and diagnosed with a Gleason score 6–7 and a clinical stage pT2–3 adenocarcinoma of the prostate were included in this study (Supplementary Table S1). To obtain a single cell suspension for FACS sorting to isolate macrophages, two isolation methods were compared: mechanical dissociation versus enzymatic digestion. The yield of CD45⁺ leukocytes and CD45⁺/CD14⁺ and/or CD11b⁺

myeloid cells was proportionally higher in mechanically digested tissue compared with enzymatically digested tissue (Supplementary Fig. S1). In addition, the percentage of live cells (DAPI-negative) was higher in mechanically digested tissue compared with enzymatically digested tissue (82.8% vs. 65.0%). This is in agreement with studies reporting loss of epitopes in immune cells, especially myeloid cells that are known to be sensitive to higher temperature (41–43). On the basis of these observations, mechanical dissociation was selected as the optimal method to isolate macrophages from the PCa samples for scRNA-seq analyses.

The procedure for obtaining native PCa-associated myeloid cells is depicted in Fig. 1A. Tissue resident macrophages were isolated from the biopsies by successively FACS sorting a single-cell suspension of the biopsies for CD45⁺ leukocytes, followed by isolation of CD3-CD14⁺ and/or CD11b⁺ myeloid cells (44–46). In total, 1,920 cells, including 911 cells isolated from the tumorous and 1,009 cells isolated from the nontumorous areas of the prostates were sequenced on eight plates (Supplementary Table S1). Cells with less than 2,000 UMIs were not considered, whereas only genes that were detected with at least four UMIs in at least three cells, were used for further analysis. In plates 4 and 7, very few cells above the 2,000 UMI cut-off were found. Furthermore, high levels of technical artefact genes like KCNQ1OT1, which is a noncoding region rich in poly-A repeats and often found in cell transcripts of poor quality were also detected (47). For these reasons, plates 4 and 7 were excluded from further analysis. The range (202–12,107) and mean (1,806) of genes (features) detected per cell are displayed in Supplementary Fig. S2A. After additional quality control filtering to remove dead, dying, or otherwise low-quality cells and cell doublets/multiplets, plate 8 was found to contain very few remaining cells and was also removed from analysis. The removal of plates 7 and 8 resulted in the loss of all cells from patient 4. Therefore, the subsequent analysis contains cells from three patients. The remaining 751 cells retained for subsequent analysis showed a range and mean of 1,026 to 5,876 and 2,787 genes per cell, respectively (Supplementary Fig. S2B).

Subsequently, the accuracy of the mpMRI to annotate tumorous and non-tumorous areas in the prostate was evaluated by histological assessments of the H&E stained prostatectomy specimen of patients 1 to 3. The presurgery mpMRI of all 3 patients, indicated areas with a high likelihood of containing tumor and an area less likely containing tumor in patient 3 correctly. In patient 1, an area less likely containing tumor was suggested, however, presence of tumor could not be confirmed (Supplementary Fig. S3). Because biopsies were taken from areas with a high likelihood of containing tumor and from areas not suspected for containing tumor in the prostate, we conclude that the biopsies were labelled correctly as “tumorous and nontumorous.”

Clustering of myeloid cells to identify PCa macrophage subtypes

To surmount the implicit noise of individual features in scRNA data, principal component (PC) analysis was used to reduce dimensionality, followed by graph-based clustering to identify populations of highly-interconnected cells (30). Initial clustering of the data yielded six independent clusters, with cluster 3 being substantially divergent from the remaining clusters (Supplementary Fig. S4A). This was also evident in the first PC (Supplementary Fig. S4B). Examination of the genes within PC1, as well as markers for various cell types across all clusters revealed that cells in cluster 3 expressed the well-known natural killer (NK) cell markers NKG7 and GNLY (Fig. 1B; Supplementary Figs. 4C and 4D; ref. 48). The presence of these cells after FACS sorting is likely residual from the CD11b (ITGAM) selection

(Fig. 1B). Because the focus of this study is macrophages, these NK cells were removed from further analysis. The 641 cells in the remaining clusters are considered macrophages as all clusters express various macrophage markers (CD68, CD86, CD163), while lacking expression of established markers for other immune cell types (T-cell, B-cell, NK-cell), prostate epithelium (FOLH1, KLK3), and mesenchymal cells (PDGFRB, FAP; Fig. 1B; refs. 49, 50).

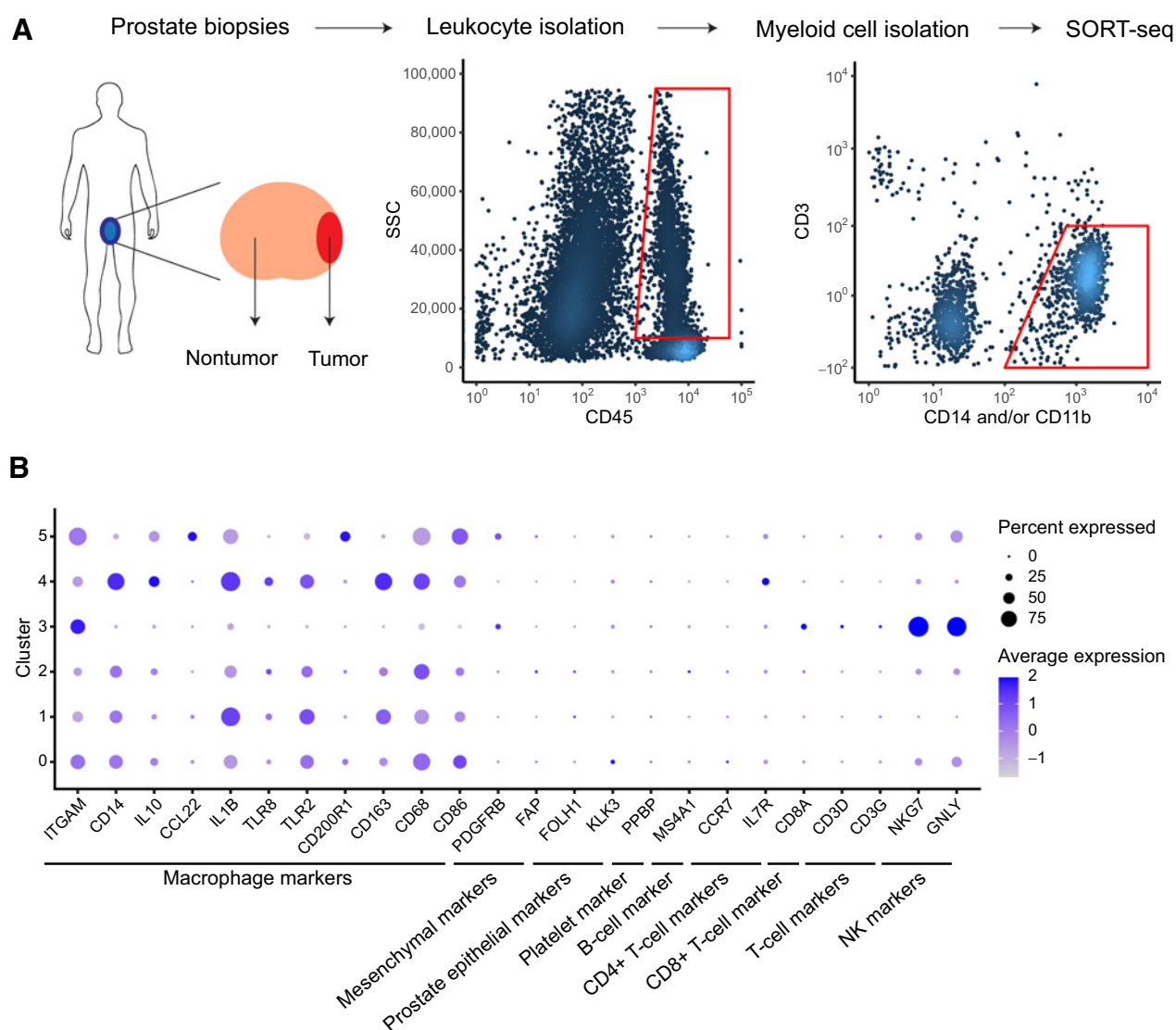
After removal of NK cells, the remaining macrophages were re-analyzed as above, and 20 PCs were selected for further analysis (Supplementary Fig. S5). Clustering these PCs yielded five populations, however the clustering was highly patient specific (Fig. 2A and B). To remove these patient-specific batch effects, a reciprocal PCA method was employed to integrate the patient datasets (see “Materials and Methods” for details). This method will effectively integrate correspondence cells between datasets even in the presence of extensive biological or technical differences (30). Clustering of the final integrated dataset revealed three distinct macrophage subtypes (Fig. 2C).

The number of macrophage clusters identified will depend on a variety of factors specific to the dataset, including the number of cells and cell types, tissue with which the macrophages are associated, method of digestion, the number of PCs used, and the resolution of the SNNs graph. The number of macrophage clusters identified in this study was largely comparable to those reported in previous scRNA-seq studies across a variety of tissues (Supplementary Table S2; refs. 51–58). The number of PCs used in this analysis were carefully selected to ensure the appropriate amount of biological variation was included (Supplementary Fig. S5). To assess the number of clusters identified, increasing resolutions for the SNN graph were tested (Supplementary Fig. S6A). This analysis indicated that while increasing the SNN resolution could force additional clusters, the new clusters were in fact subclusters of the three primary subtypes, and no new distinct clusters were identified. While the primary subtypes may indeed have subclusters of specific function, this analysis revealed that subclusters were often defined by a relatively small number of cells or genes in this dataset, and appeared unstable as they often merged back together at different resolutions. Therefore, in this study we focused only on the three primary macrophage subtypes identified.

In the integrated dataset, the cells from each patient were no longer forming isolated or dominant clusters, but were instead distributed across all three clusters, indicating that the reciprocal PCA method was effective at removing the patient-specific batch effects (Figs. 2D). Unexpectedly, the macrophages from the tumor and nontumorous biopsies showed nearly identical distributions among the clusters, and no differences were observed between the macrophage subtypes present in the tumorous and nontumorous portions of the diseased prostate (Figs. 2E and F). In addition, the distributions of CD11b (ITGAM) and CD14 expressing cells were assessed in the three clusters and found to be comparable between the tumorous and nontumorous cells (Supplementary Fig. S6B). Cumulatively, these results indicate that there are three biologically distinct macrophage subtypes present in the tumorous and nontumorous portions of diseased human prostates.

Evaluation of M1 and M2 macrophage phenotypes in PCa clusters

As a first step to examine the identity of these macrophage clusters, previously established markers associated with M1-like and M2-like phenotypes were investigated (24). Plotting all detectable M1 and M2 marker genes for each cell in a heatmap revealed that many markers are not readily detectable in all cells and there is no clear M1/M2

**Figure 1.**

Single cell sequencing of myeloid cells from patients with PCa. **A**, Experimental procedure: single cell suspensions of multiple biopsies from the tumor and tumor-adjacent portions of RP specimens were sequentially FACS sorted to isolate $CD45^+/CD14^+$ and/or $CD45^+/CD11b^+$ myeloid cells, after negative selection for $CD45^+CD3^+$ lymphocytes. Subsequently, single cells were processed for SORT-seq analysis. **B**, Dot plot for average expression levels of markers for macrophages, other immune cells, and prostate cell types present in the clusters. Cells were positively identified as macrophages and NK cells.

separation between these clusters (Fig. 3A). Given the varying expression levels and the sparsity of marker expression, averaging individual markers within each cluster was not useful in evaluating M1/M2 identity within the clusters, though it appeared that M2 markers were generally expressed at higher levels (Supplementary Figs. S7A and S7B). For these reasons, all M1 and M2 markers were separately combined by averaging the RNA expression of all M1 or M2 markers within each cell. From this analysis it is evident that the mean expression level of all combined M2 markers per cell are higher than the mean M1 marker expression levels (Fig. 3B; Supplementary Fig. S7C). Furthermore, the mean M1 expression levels were slightly but significantly higher in cluster 2, while the mean M2 expression levels were significantly elevated in cluster 0 (Fig. 3C and D). These results demonstrate that although a slightly elevated expression of the

averaged M1 and M2 markers can be detected in certain clusters, these are not the main factors contributing to the variation that separates these macrophage populations.

Identification of differentially expressed genes and biological pathways

To determine the biological differences between these three macrophage clusters, differential expression analysis was performed to detect marker genes in each cluster. This analysis identified 468 significantly differentially expressed genes, with 164 genes identified as markers in cluster 0, 199 genes in cluster 1, and 105 genes in cluster 2 (Supplementary Table S3). Examining this list of genes showed only 11/68 M1 and M2 markers to be differentially expressed, with 3/33 M1 markers upregulated in cluster 2 and 6/35 M2 markers upregulated in

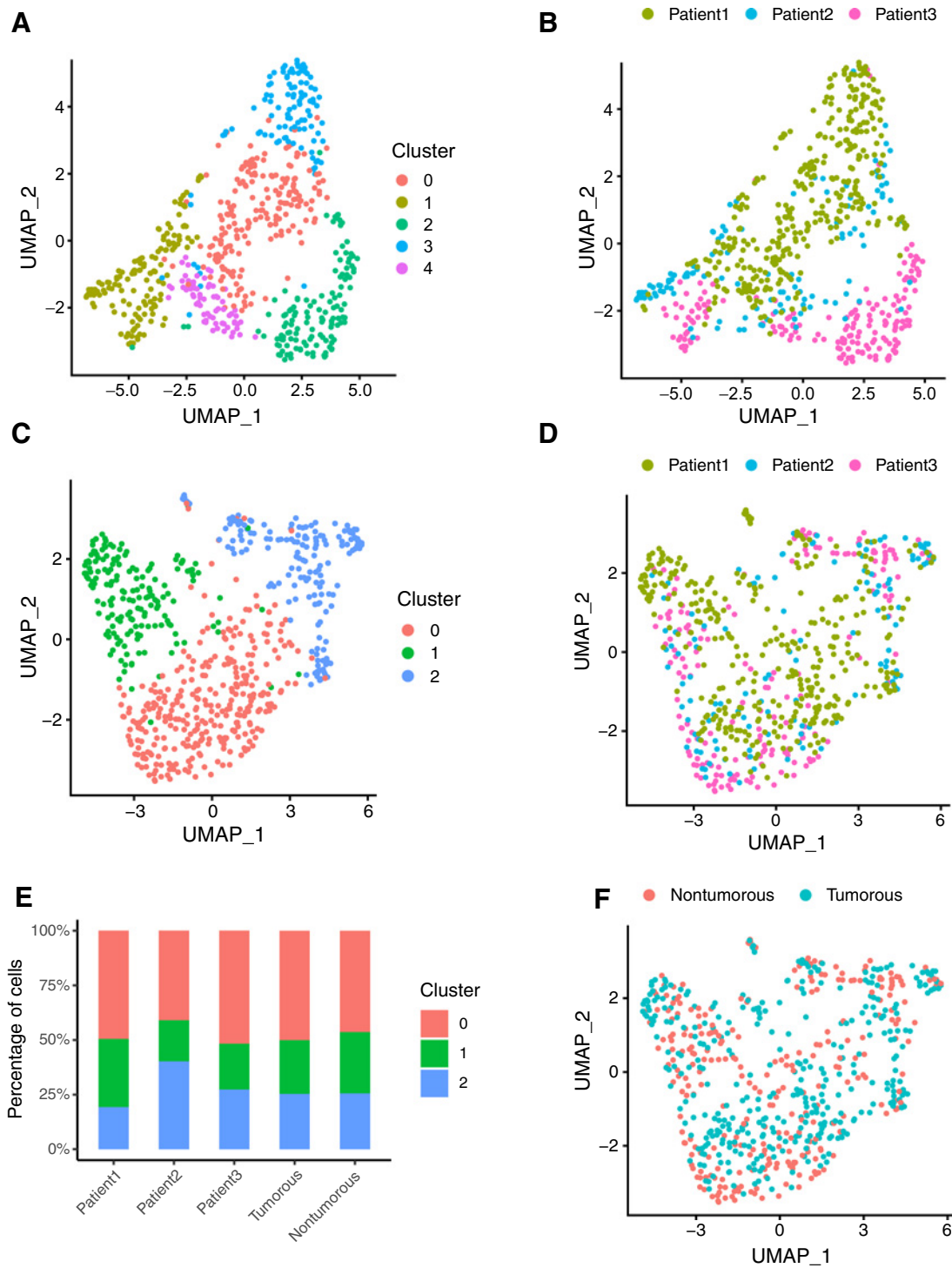


Figure 2. Identification of PCa-associated macrophage subtypes. **A**, UMAP projections of macrophage clustering after NK-cell removal. Colors indicate five distinct clusters. **B**, UMAP projections of cells from each patient reveals strong patient-specific batch effects. Each color represents cells from a different patient. **C**, UMAP projections after reciprocal-PCA integration removing batch effects between patients. Colors indicate three distinct clusters. **D**, UMAP projection of integrated data shows all patient samples are comparable and do not cluster separately. Each color represents cells from a different patient. **E**, Distributions of cells within each cluster, with percentage of cells from each cluster show on the y-axis. **F**, UMAP projection of macrophages isolated from tumor (pink) and tumor adjacent (blue-green) biopsies are comparable and do not cluster separately.

Downloaded from <http://aacrjournals.org/mcr/article-pdf/19/10/1778/2967699/1778.pdf> by guest on 16 February 2022

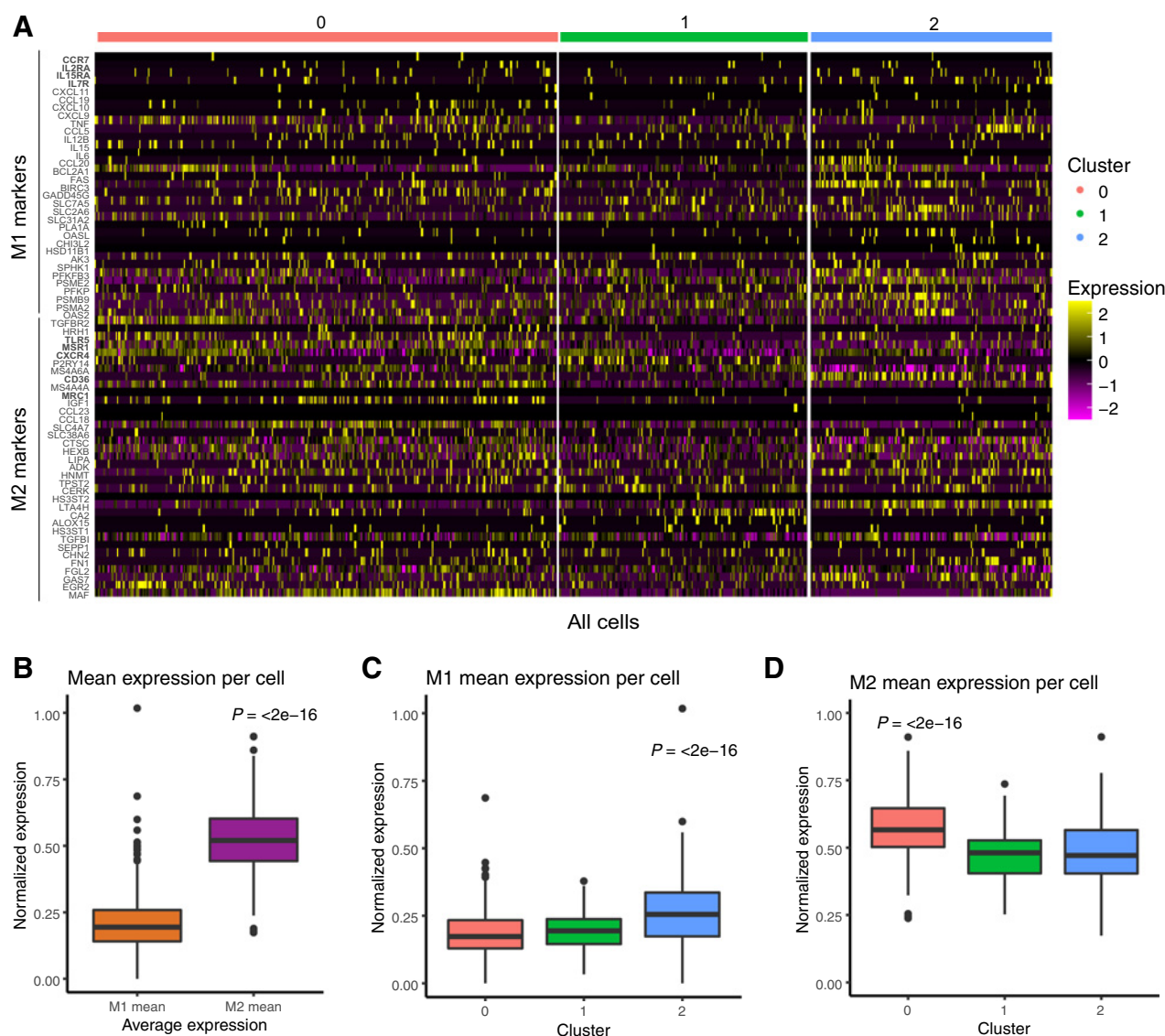


Figure 3.

Canonical M1 and M2 macrophage marker expression in PCa associated macrophages. **A**, Heatmap of all detectable canonical markers used to differentiate M1 and M2 macrophages by gene expression in relation to the three macrophage clusters. Cell surface markers are highlighted in bold. Color bar indicates RNA expression level scaled by z-score. **B**, Mean expression of all M1 (orange) or M2 (purple) markers from **A** averaged together within each cell. P values from Welch t test. **C**, Average normalized expression of all M1 markers in **A** per cell within each cluster. P values from one-way ANOVA with *post hoc* Tukey HSD. **D**, Average normalized expression of all M2 markers in **A** per cell within each cluster; P values from one-way ANOVA with *post-hoc* Tukey HSD.

cluster 0 (Supplementary Table S4). These results agree with the slight enrichments observed in **Fig. 3C** and **D**, however there are also two M2 markers upregulated in cluster 2, further exemplifying the need for better stratification. The most differentially expressed genes from each cluster show either expression only in their cluster, or elevated expression as compared with the other clusters (**Fig. 4**). These genes represent ideal markers for these novel macrophage subtypes.

To evaluate the localization of macrophage subtypes in prostatectomy samples, we scored IHC staining of a representative ideal marker from each macrophage cluster, as well as a pan-macrophage marker (CD68), in multiple independent patient samples (Supplementary Fig. S8; ref. 59). Analysis of CD68 control, SLC40A1 for cluster 0, PLAC8 for cluster 1, and FCN1 for cluster 2 suggested that the three

macrophage subtypes are present in both the tumorous and nontumorous portions of PCa patient samples at approximately equal percentages (Supplementary Figs. S9A–S9D). When correcting for the overall percentage of tumor, the density of CD68 and PLAC8 (Cluster 1) positive cells was higher in the nontumorous portions of the prostatectomy samples than in the tumorous portions, whereas there was no difference in density of SLC40A1 (Cluster 0) and FCN1 (Cluster 2) positive cells between the two portions (Supplementary Fig. S9E).

To explore the functional pathways that genes associated with each cluster are involved in, GSEA was performed (Supplementary Fig. S10). Cluster 0 genes showed activation of the hallmark TNF α signaling via NFKB as well as WNT β -catenin signaling, and

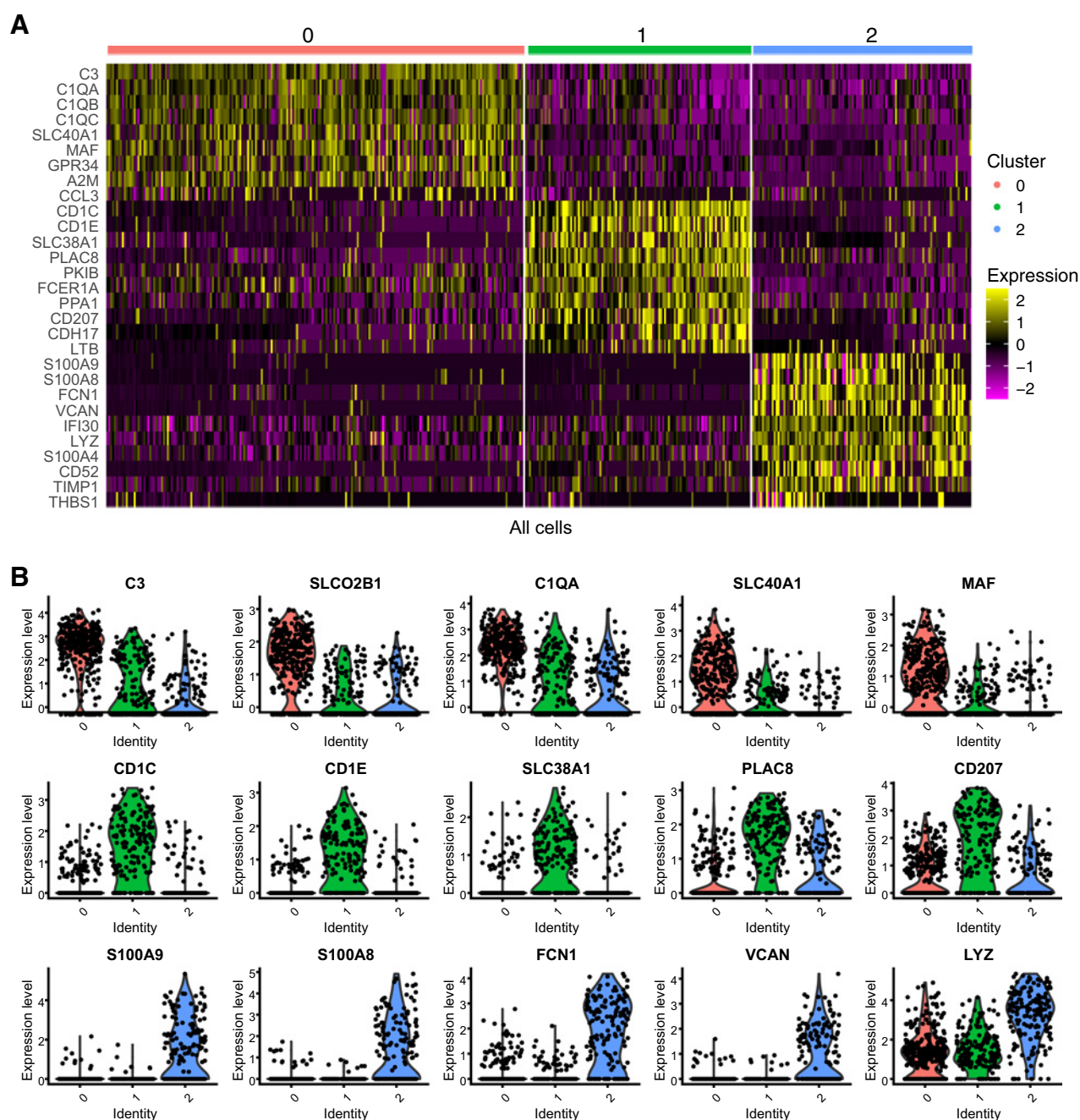


Figure 4.

Identification of marker genes for each macrophage cluster. **A**, Heatmap of the top 10 most differentially expressed genes in each macrophage cluster with expression level scaled to z-score. **B**, Violin plots for the top 5 most differentially expressed genes in each cluster showing normalized RNA expression levels. Colors indicate macrophage clusters and each black dot represents a cell.

suppression of interferon pathways (IFN α and IFN γ), MTORC1 signaling, and complement pathways, among others (Supplementary Fig. S10A). Conversely, cluster 2 showed activation of multiple inflammatory pathways including IFN α , IFN γ , TNF α , and complement, while showing suppression of WNT β -catenin signaling and cell-cycle pathways (Supplementary Fig. S10B). Cluster 1, however, showed suppression of multiple immune pathways (IFN α , IFN γ , TNF α , among others), and activation of cell-cycle pathways (E2F

targets, MYC targets, G2M checkpoint) as well as MTORC1 signaling (Supplementary Fig. S10C). To explore the possibility of PCa TAM regulation of T cells, known markers of T-cell regulation by TAMs were interrogated in the data (60). Very few of these markers were readily detectable and only one, CSF1R, was found to be significantly differentially expressed (Supplementary Fig. S11). Collectively, these results suggest that each macrophage population is involved in unique biological functions.

Generation and evaluation of macrophage gene signature

To develop a prospective gene signature, all genes in the integrated dataset found to be significantly differentially expressed between macrophage clusters were included in the model (Fig. 5A). Using a published PCa dataset from Memorial Sloan Kettering Cancer Center (MSKCC) (34), a 217-gene prognostic signature (Supplementary Table S5) predicting biochemical RFS of patients with PCa was selected (see “Materials and Methods” for details). The performance of the macrophage gene signature was evaluated employing 10-fold nested cross-validation on the MSKCC dataset using ROC as a performance measure (Fig. 5B). As expected, in a Cox regression analysis this classifier showed a significant association with RFS (HR = 4.1; $P = 1.7e-05$; Fig. 5C). Furthermore, in a multivariate analysis including the signature with Gleason score (biopsy and pathologic), prediagnosis biopsy PSA levels, seminal vesicle invasion (SVI), extracapsular extension (ECE), and clinical stage the signature was found to be an independent predictor of outcome (Fig. 5D).

Using the Cox model linear predictor as a prognostic index (PI), the relative prognostic value of each macrophage cluster was assessed by summing the product of the model coefficients (β s) and the scaled gene expression values in each cell (Supplementary Fig. S12). This analysis demonstrated that cells from cluster 2 had a low PI, while cells from clusters 0 and 1 had a high PI. This result indicates that higher numbers of cells from cluster 2 are associated with better outcome, whereas higher numbers of cells from clusters 0 and 1 are associated with worse outcome. Taken together with the pathway analysis in Supplementary Fig. S10, these results indicate that the pro-inflammatory macrophage subsets are associated with better outcome, whereas anti-inflammatory and proliferative macrophage subtypes are associated with worse outcome.

Validation of gene signature in independent PCa cohorts

To further assess the prognostic value of the macrophage gene signature, it was validated in three independent cohorts from the Decipher GRID registry. The first cohort is a prospective Decipher GRID cohort containing RNA expression data from >5,000 patients with RP and includes basic demographic and pathologic data, but not longitudinal clinical outcomes. This cohort was used to associate the signature to Decipher risk groups and pathologic Gleason score (Fig. 6A and B). Because this cohort has no metastasis outcome yet, high Decipher group was used as a surrogate of metastasis potential since it was heavily validated for that endpoint (38, 40, 61). The second cohort is a retrospective natural history cohort ($n = 355$) comprised of men treated with RP at Johns Hopkins Medical Institutions (JHMI) (38). The third cohort is a retrospective cohort ($n = 780$) of men treated with RP at the Mayo Clinic (40, 61). All three cohorts are described in Supplementary Table S6.

The strength of association of the macrophage signature with metastasis-free survival was tested using a Cox regression analysis on the Mayo and JHMI cohorts and the signature showed significant association with metastasis-free survival (Mayo: HR = 1.89, P value = $1.0e-06$; JHMI: HR = 2.25, P value = $3.3e-05$; Fig. 6C and D). In both cohorts, the classifier was also found to be an independent predictor of metastasis in multivariate analysis (Supplementary Table S7). Taken together, these results indicate that profiling single-cell RNA expression in PCa-associated macrophages and identifying subpopulations present in the diseased prostate can have significant prognostic value in predicting patients' likelihood of biochemical relapse and metastasis. These results lay the foundation for profiling macrophage populations in PCa and other cancer types, and will inform future studies investigating the immune systems' role in cancer progression.

Discussion

Macrophages can either promote or suppress cancer development and progression depending on their specific phenotype and function. In this study, we defined the degree of human PCa-specific macrophage diversity through single-cell sequencing with the aim to identify PCa-specific macrophage populations. Three macrophage subtypes were identified, and although some canonical M1 and M2 markers were present, these were not adequate to define the clusters. The distinction between inflammatory M1 and anti-inflammatory/proliferative M2 macrophages was based on *in vitro* cell line models and describe the two extremes of the spectrum of macrophage differentiation (21). Our findings suggest that the M1/M2 distinction of macrophage differentiations does not accurately recapitulate native PCa associated macrophages, which should be considered in future studies.

Our results are largely in line with a recent single-cell study describing cell types in human PCa (58). Here the authors showed evidence that TAMs express a mixture of M1 and M2 markers, and that two of the main sources of variation between TAM subtypes are TNF α and NF κ B pathways. This study identified five macrophage clusters, suggesting that surveying more patients and sequencing higher numbers of cells may further our understanding of the role TAMs play in PCa. Of note for comparison of our study with previous studies, are the different methods of obtaining single cell solutions. Although most previous studies performed enzymatic digestion, we performed mechanical dissociation. This difference in techniques, might introduce a bias for particular cell populations. However, in agreement with previous studies (41–43), we demonstrated that mechanical digestion leads to a higher number of live myeloid cells as compared with enzymatic digestion. This becomes particularly relevant in poorly infiltrated tumors, such as PCa, where the immune cell content, specifically macrophages, is already reduced.

Multiple reports demonstrated a correlation between TAMs and poor prognosis of patients with PCa (62–64); however, the vast majority of these studies only focused on a small selection of TAM-associated markers, including IL10, CD163, and MRC1 (CD206). Other than previous studies, we constructed signatures and clustering of macrophages based on the transcriptional profile of macrophages as they occur in all their complexity in the human PCa-microenvironment. Using the genes differentially expressed between the clusters, we were able to develop a gene signature with significant prognostic value in multiple independent PCa cohorts. These results advance the field not only by defining TAMs subtypes, but also by demonstrating that the genes differentially expressed between these subtypes can predict a PCa patient's prognostic outlook in terms of biochemical recurrence and metastasis.

Macrophages were isolated from biopsies from the “tumorous” and “nontumorous” sites of the prostate. Sites of the biopsies were identified using presurgery mpMRI images. Although the presence of tumor was not histologically confirmed in the biopsies themselves, histologic evaluation of the whole prostatectomy specimen confirmed that the mpMRI images correctly identified tumorous areas in all three patients. This confirms correct labelling of biopsies as tumorous or nontumorous. Remarkably, no differences were observed between macrophage subtypes found in the tumorous and the nontumorous sites, suggesting that tumorigenic factors may also affect distant nontumorigenic sites. Furthermore, this suggests that these macrophage populations could in theory be detected from a biopsy regardless to tumor cell percentage. This is important because the prognostic value of the gene signature outweighs the biopsy Gleason

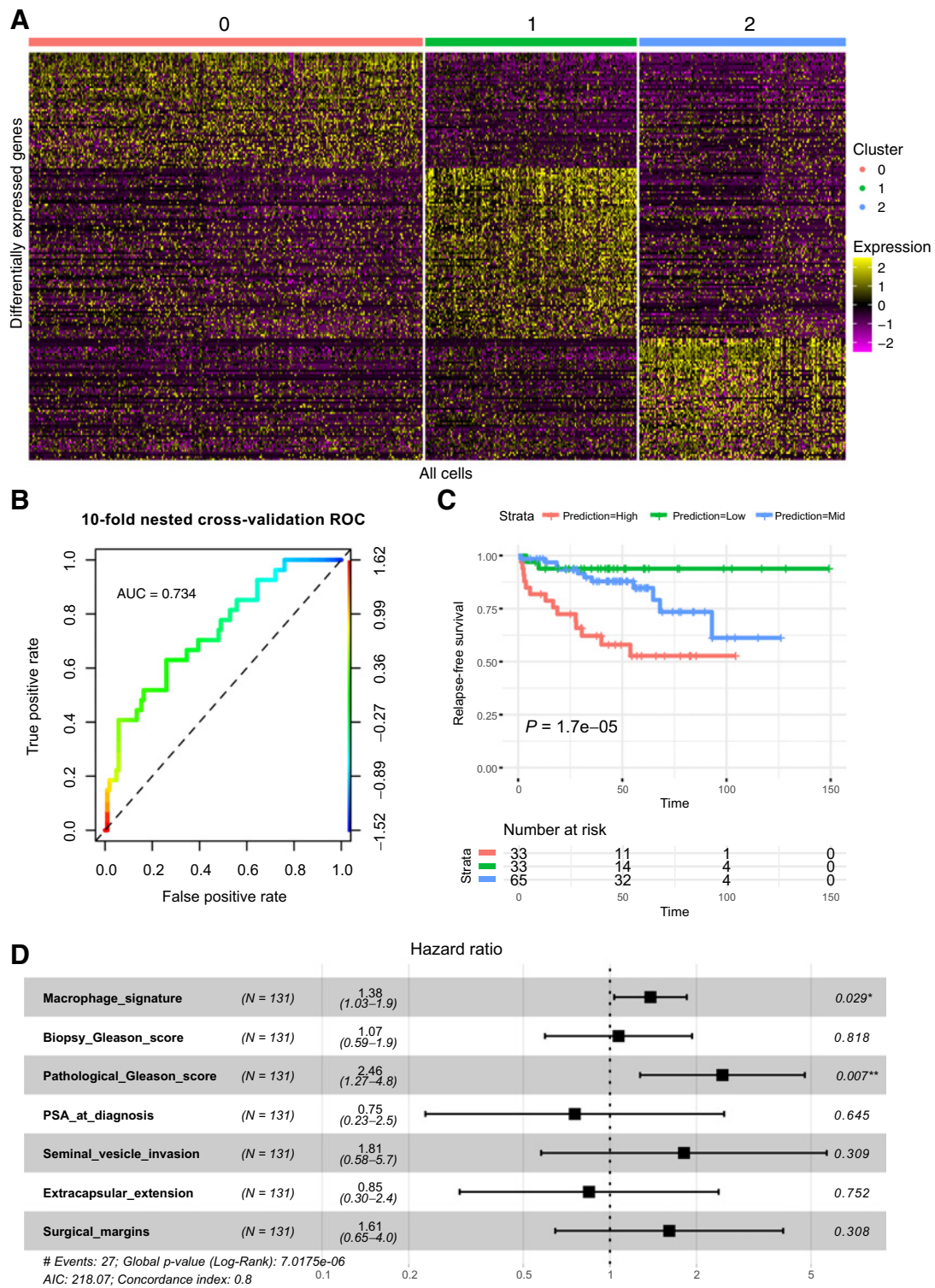
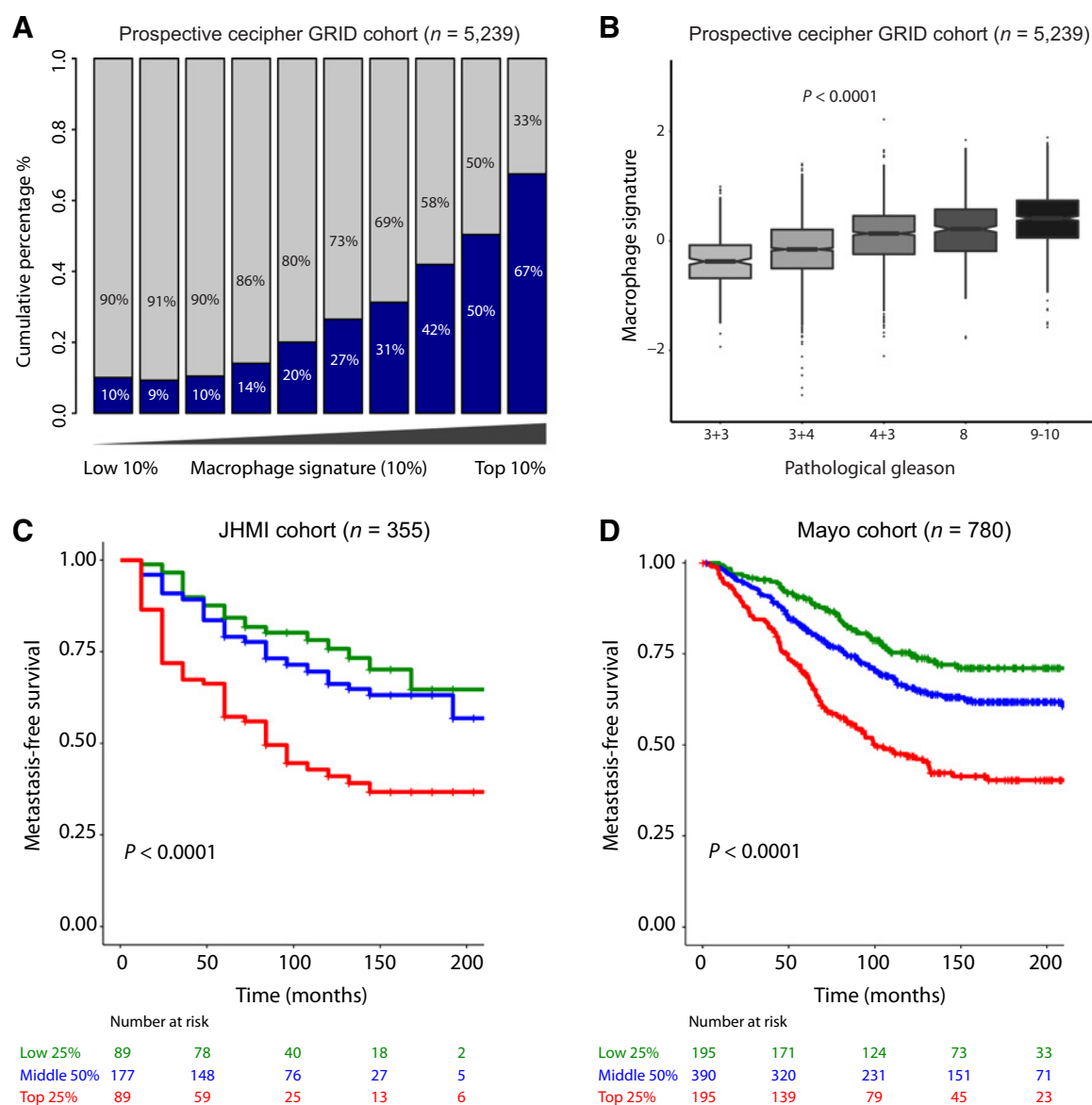


Figure 5.

Gene signature from differentially expressed macrophage genes has significant prognostic value. **A**, Heatmap of all significant differentially expressed genes present in the integrated dataset by macrophage cluster (Bonferroni adjusted P value <0.05). Color bar indicates integrated expression level scaled by z-score. **B**, ROC curve for 10-fold cross-validation of macrophage signature in MSKCC dataset, colored by threshold value. **C**, Macrophage gene signature outcome predictions from 10-fold cross-validation in MSKCC dataset. Colors indicate patient subpopulations of predicted high (red; 25%), medium (blue; 50%), and low (green; 25%) risk of recurrence. P value is from log-rank test. **D**, Multivariate Cox regression analysis for macrophage signature in MSKCC cohort showing HR with 95% CI and P value from log-rank test.

**Figure 6.**

Validation of the gene signature in independent PCa cohorts. **A**, Macrophage gene signature predictions correlate in a prospective cohort of >5,000 patients with high Decipher GRID scores (blue) versus low and intermediate scores (gray). **B**, Macrophage gene signature predictions correlate with pathologic Gleason score in Decipher GRID. P value from linear model between Gleason and Macrophage signature. **C** and **D**, Gene signature outcome predictions in two independent PCa cohorts from JHMI (**C**) and Mayo Clinic (**D**), stratifying patients on low (green, bottom 25%), medium (blue; middle 50%), or high (red; top 25%) risk of metastatic disease. Y-axis shows metastasis-free survival, number of patients at risk are indicated, P values from log-rank test.

score and pre-diagnosis biopsy PSA levels, and is approaching the significance of pathological Gleason, suggesting a possible path to identifying high-risk patients without necessitating RP. In addition, the macrophage signature and pathological Gleason score were both independent predictors in our multivariate analysis, suggesting that the signature can provide additional prognostic information. However, these findings will require further experimental validation before such measures could be employed.

The GSEA performed in this study suggests that each macrophage subtype is involved in unique biological processes. Cluster 1 does not appear to be participating in inflammatory pathways and may represent a proliferative feeder cell type, or otherwise less differentiated

macrophage subtype. Cluster 0 appears to be largely anti-inflammatory, whereas cluster 2 appears primarily pro-inflammatory. These results agree with the notion that macrophages can broadly adopt either a pro-inflammatory or anti-inflammatory phenotype, and this could either potentiate or mediate cancer progression (6, 7, 24). Moreover, because there was no difference in the occurrence of the three clusters in biopsies from the tumorous and nontumorous site of the prostate, the differences in functions of the macrophages in the three clusters may be related to the origin of the macrophages, which could either be embryonic-derived or blood-derived (4).

Furthermore, using a PI we demonstrate that pro-inflammatory cluster 2 cells are associated with better prognosis, whereas the

anti-inflammatory cluster 0 and anti-inflammatory/proliferative cluster 1 cells are associated with worse outcome. These suggest that targeting cluster 2 cells to increase their numbers and targeting clusters 0 and 1 to decrease their numbers is a potential therapeutic strategy for patients with PCa. To this purpose, our findings provide novel drug targetable genes specific for each cluster. It will be important for future studies to explore the role these macrophage populations play in PCa, and to investigate targeting these subtypes and their associated pathways with immunotherapy.

Cancer immunotherapies, specifically those inhibiting T-cell immune checkpoints, have generated significant impact in recent years, with established efficacy in advanced melanoma (65, 66), non-small cell lung cancer (67, 68) and bladder cancer patients (69, 70). However, in other cancers, including PCa, immunotherapy efficacy is limited (71, 72). The uncertain therapeutic efficacy of immunotherapy in PCa is partly due to a poor infiltration of immune cells in the TME (16, 73–76). Moreover, TAMs display an ability to modulate tumor immunity by suppression of T-cell recruitment and function, although the precise mechanisms have yet to be elucidated (60). Several direct and indirect suppressive actions of macrophages on T-cell functions have been suggested, including involvement of immune checkpoints ligands (e.g., PDL1, B7-H4), cytokines (e.g., IL10, CXCL10, CCL22), and cell surface receptors (e.g., CD2017, CSF1R; ref. 60). However, in this study, only the colony-stimulating factor 1 receptor (CSF1R), which is a key regulator of immunosuppressive macrophage expansion, was found to be enriched in cluster 0. Whether the macrophage subtypes discovered in this study play a role in T-cell regulation will be an important question for future studies.

Limitations of this study include the small number of patients included in the study and the absence of assessment of protein expression of the key selected genes. To this end, future studies should include immunohistochemistry analysis to further support our findings.

In conclusion, in this study we demonstrate the relevance of using single-cell transcriptomics from PCa-associated macrophages as a

prognostication strategy for individual patients. We propose that targeting unique tumor-associated macrophage subtypes, as opposed to all macrophages, can provide a therapeutic avenue to combat PCa and potentially other cancer types.

Authors' Disclosures

F.Y. Feng reports personal fees from Janssen, Blue Earth Diagnostics, Astellas, Myovant, Roivant, Genentech, Bayer, PFS Genomics, SerImmune, and Bristol-Myers Squibb outside the submitted work. L.F.A. Wessels reports grants from Genmab BV during the conduct of the study. W. Zwart reports grants from Astellas Pharma outside the submitted work. A.M. Bergman reports grants from FP7 MCA-ITN and KWF Dutch Cancer Society during the conduct of the study. No disclosures were reported by the other authors.

Authors' Contributions

J.C. Siefert: Formal analysis, investigation, visualization, methodology, writing—original draft, writing—review and editing. B. Cioni: Conceptualization, investigation, writing—original draft, writing—review and editing. M.J. Muraro: Conceptualization, resources, data curation, formal analysis, writing—original draft. M. Alshalalfa: Formal analysis, validation, visualization, writing—original draft. J. Vivie: Resources, data curation, investigation. H.G. van der Poel: Resources, writing—review and editing. I.G. Schoots: Visualization. E. Bekers: Visualization. F.Y. Feng: Resources, supervision. L.F.A. Wessels: Resources, supervision, writing—review and editing. W. Zwart: Resources, supervision, writing—review and editing. A.M. Bergman: Conceptualization, resources, supervision, funding acquisition, writing—original draft, writing—review and editing.

Acknowledgments

We thank our collaborators from Single Cell Discoveries B.V., supported by the Hubrecht Institute and the Oncode Institute. This work was supported by the FP7 MCA-ITN grant agreement 317445 – TIMCC and KWF Dutch Cancer Society grant No. 2009–4356 awarded to Andre Bergman.

The costs of publication of this article were defrayed in part by the payment of page charges. This article must therefore be hereby marked *advertisement* in accordance with 18 U.S.C. Section 1734 solely to indicate this fact.

Received August 26, 2020; revised December 18, 2020; accepted June 7, 2021; published first June 15, 2021.

References

- Davies LC, Jenkins SJ, Allen JE, Taylor PR. Tissue-resident macrophages. *Nat Immunol* 2013;14:986–95.
- Ginhoux F, Greter M, Leboeuf M, Nandi S, See P, Gokhan S, et al. Fate mapping analysis reveals that adult microglia derive from primitive macrophages. *Science* 2010;330:841–5.
- Hashimoto D, Chow A, Noizat C, Teo P, Beasley MB, Leboeuf M, et al. Tissue-resident macrophages self-maintain locally throughout adult life with minimal contribution from circulating monocytes. *Immunity* 2013;38:792–804.
- Epelman S, Lavine KJ, Randolph GJ. Origin and functions of tissue macrophages. *Immunity* 2014;41:21–35.
- Gordon S, Pluddemann A, Martinez Estrada F. Macrophage heterogeneity in tissues: phenotypic diversity and functions. *Immunol Rev* 2014;262:36–55.
- Beyer M, Mallmann MR, Xue J, Staratschek-Jox A, Vorholt D, Krebs W, et al. High-resolution transcriptome of human macrophages. *PLoS One* 2012;7:e45466.
- Xue J, Schmidt SV, Sander J, Draffehn A, Krebs W, Quester I, et al. Transcriptome-based network analysis reveals a spectrum model of human macrophage activation. *Immunity* 2014;40:274–88.
- Müller S, Kohanbash G, Liu SJ, Alvarado B, Carrera D, Bhaduri A, et al. Single-cell profiling of human gliomas reveals macrophage ontogeny as a basis for regional differences in macrophage activation in the tumor microenvironment. *Genome Biol* 2017;18:234.
- Xue D, Tabib T, Morse C, Lafyatis R. Single-cell RNA sequencing reveals different subsets of macrophage and dendritic cells in human skin. *J Immunol* 2019;202(1 Supplement):177.8.
- Zhang Q, He Y, Luo N, Patel SJ, Han Y, Gao R, et al. Landscape and dynamics of single immune cells in hepatocellular carcinoma. *Cell* 2019;179:829–45.
- Poltavets V, Kochetkova M, Pitson SM, Samuel MS. The role of the extracellular matrix and its molecular and cellular regulators in cancer cell plasticity. *Front Oncol* 2018;8:431.
- Mantovani A, Marchesi F, Malesci A, Laghi L, Allavena P. Tumour-associated macrophages as treatment targets in oncology. *Nat Rev Clin Oncol* 2017;14:399–416.
- Poh AR, Ernst M. Targeting macrophages in cancer: from bench to bedside. *Front Oncol* 2018;8:49.
- Lanciotti M, Masieri L, Raspollini MR, Minervini A, Mari A, Comito G, et al. The role of M1 and M2 macrophages in prostate cancer in relation to extracapsular tumor extension and biochemical recurrence after radical prostatectomy. *Biomed Res Int* 2014;2014:486798.
- Shimura S, Yang G, Ebara S, Wheeler TM, Frolov A, Thompson TC. Reduced infiltration of tumor-associated macrophages in human prostate cancer: association with cancer progression. *Cancer Res* 2000;60:5857–61.
- Nonomura N, Takayama H, Nakayama M, Nakai Y, Kawashima A, Mukai M, et al. Infiltration of tumour-associated macrophages in prostate biopsy specimens is predictive of disease progression after hormonal therapy for prostate cancer. *BJU Int* 2011;107:1918–22.
- Hu W, Qian Y, Yu F, Liu W, Wu Y, Fang X, et al. Alternatively activated macrophages are associated with metastasis and poor prognosis in prostate adenocarcinoma. *Oncol Lett* 2015;10:1390–6.

18. Gollapudi K, Galet C, Grogan T, Zhang H, Said JW, Huang J, et al. Association between tumor-associated macrophage infiltration, high grade prostate cancer, and biochemical recurrence after radical prostatectomy. *Am J Cancer Res* 2013;3: 523–9.
19. Escamilla J, Schokrpur S, Liu C, Priceman SJ, Moughon D, Jiang Z, et al. CSF1 receptor targeting in prostate cancer reverses macrophage-mediated resistance to androgen blockade therapy. *Cancer Res* 2015;75:950–62.
20. Xu J, Escamilla J, Mok S, David J, Priceman S, West B, et al. CSF1R signaling blockade stanches tumor-infiltrating myeloid cells and improves the efficacy of radiotherapy in prostate cancer. *Cancer Res* 2013;73:2782–94.
21. Wong D, Kandagatla P, Korz W, Chinni SR. Targeting CXCR4 with CTCE-9908 inhibits prostate tumor metastasis. *BMC Urol* 2014;14:12.
22. Huang EH, Singh B, Cristofanilli M, Gelovani J, Wei C, Vincent L, et al. A CXCR4 antagonist CTCE-9908 inhibits primary tumor growth and metastasis of breast cancer. *J Surg Res* 2009;155:231–6.
23. Higano CS, Schellhammer PF, Small EJ, Burch PA, Nemunaitis J, Yuh L, et al. Integrated data from 2 randomized, double-blind, placebo-controlled, phase 3 trials of active cellular immunotherapy with sipuleucel-T in advanced prostate cancer. *Cancer* 2009;115:3670–9.
24. Martinez FO, Gordon S. The M1 and M2 paradigm of macrophage activation: time for reassessment. *F1000Prime Rep* 2014;6:13.
25. Norström MM, Rådestad E, Stikvoort A, Egevad L, Bergqvist M, Henningsohn L, et al. Novel method to characterize immune cells from human prostate tissue. *Prostate* 2014;74:1391–9.
26. Muraro MJ, Dharmadhikari G, Grün D, Groen N, Dielen T, Jansen E, et al. A single-cell transcriptome atlas of the human pancreas. *Cell Syst* 2016;3:385–94.
27. van den Brink SC, Sage F, Vértésy Á, Spanjaard B, Peterson-Maduro J, Baron CS, et al. Single-cell sequencing reveals dissociation-induced gene expression in tissue subpopulations. *Nat Methods* 2017;14:935–6.
28. Hashimshony T, Senderovich N, Avital G, Klochendler A, de Leeuw Y, Anavy L, et al. CEL-Seq2: sensitive highly-multiplexed single-cell RNA-seq. *Genome Biol* 2016;17:77.
29. Grun D, Kester L, van Oudenaarden A. Validation of noise models for single-cell transcriptomics. *Nat Methods* 2014;11:637–40.
30. Stuart T, Butler A, Hoffman P, Hafemeister C, Papalexi E, Mauck WM, et al. Comprehensive integration of single-cell data. *Cell* 2019;177:1888–902.
31. Chung NC, Storey JD. Statistical significance of variables driving systematic variation in high-dimensional data. *Bioinformatics* 2015;31:545–54.
32. Zappia L, Oshlack A. Clustering trees: a visualization for evaluating clusterings at multiple resolutions. *Gigascience* 2018;7:giy083.
33. Yu G, Wang LG, Han Y, He QY. clusterProfiler: an R package for comparing biological themes among gene clusters. *OMICS* 2012;16:284–7.
34. Taylor BS, Schultz N, Hieronymus H, Gopalan A, Xiao Y, Carver BS, et al. Integrative genomic profiling of human prostate cancer. *Cancer Cell* 2010;18: 11–22.
35. Friedman J, Hastie T, Tibshirani R. Regularization paths for generalized linear models via coordinate descent. *J Stat Softw* 2010;33:1–22.
36. Terry M, Therneau PMG. Modeling survival data: extending the Cox model, in Springer. Springer: New York; 2000.
37. Sing T, Sander O, Beerenwinkel N, Lengauer T. ROCr: visualizing classifier performance in R. *Bioinformatics* 2005;21:3940–1.
38. Ross AE, Johnson MH, Yousefi K, Davicioni E, Netto GJ, Marchionni L, et al. Tissue-based genomics augments post-prostatectomy risk stratification in a natural history cohort of intermediate- and high-risk men. *Eur Urol* 2016;69: 157–65.
39. Erho N, Crisan A, Vergara IA, Mitra AP, Ghadessi M, Buerki C, et al. Discovery and validation of a prostate cancer genomic classifier that predicts early metastasis following radical prostatectomy. *PLoS One* 2013;8:e66855.
40. Karnes RJ, Bergstralh EJ, Davicioni E, Ghadessi M, Buerki C, Mitra AP, et al. Validation of a genomic classifier that predicts metastasis following radical prostatectomy in an at risk patient population. *J Urol* 2013;190:2047–53.
41. Autengruber A, Gereke M, Hansen G, Hennig C, Bruder D. Impact of enzymatic tissue disintegration on the level of surface molecule expression and immune cell function. *Eur J Microbiol Immunol* 2012;2:112–20.
42. Ford AL, Foulcher E, Goodsall AL, Sedgwick JD. Tissue digestion with dispase substantially reduces lymphocyte and macrophage cell-surface antigen expression. *J Immunol Methods* 1996;194:71–5.
43. Chen Z, Chen X, Xu Y, Xiong P, Fang M, Tan Z, et al. Collagenase digestion down-regulates the density of CD27 on lymphocytes. *J Immunol Methods* 2014; 413:57–61.
44. Perera PY, Mayadas TN, Takeuchi O, Akira S, Zaks-Zilberman M, Goyert SM, et al. CD11b/CD18 acts in concert with CD14 and Toll-like receptor (TLR) 4 to elicit full lipopolysaccharide and taxol-inducible gene expression. *J Immunol* 2001;166:574–81.
45. Lasitschka F, Giese T, Paparella M, Kurzhals SR, Wabnitz G, Jacob K, et al. Human monocytes downregulate innate response receptors following exposure to the microbial metabolite n-butyrate. *Immun Inflamm Dis* 2017;5:480–92.
46. da Silva TA, Zorzetto-Fernandes ALV, Cecilio NT, Sardinha-Silva A, Fernandes FF, Roque-Barreira MC. CD14 is critical for TLR2-mediated M1 macrophage activation triggered by N-glycan recognition. *Sci Rep* 2017;7:7083.
47. Zhu S, Zhang XO, Yang L. Panning for long noncoding RNAs. *Biomolecules* 2013;3:226–41.
48. Butler A, Hoffman P, Smibert P, Papalexi E, Satija R. Integrating single-cell transcriptomic data across different conditions, technologies, and species. *Nat Biotechnol* 2018;36:411–20.
49. Sugimoto H, Mundel TM, Kieran MW, Kalluri R. Identification of fibroblast heterogeneity in the tumor microenvironment. *Cancer Biol Ther* 2006;5:1640–6.
50. Fearon DT. The carcinoma-associated fibroblast expressing fibroblast activation protein and escape from immune surveillance. *Cancer Immunol Res* 2014;2: 187–93.
51. Taylor SA, Chen SY, Gadhvi G, Feng L, Gromer KD, Abdala-Valencia H, et al. Transcriptional profiling of pediatric cholestatic livers identifies three distinct macrophage populations. *PLoS One* 2021;16:e0244743.
52. Evren E, Ringqvist E, Tripathi KP, Sleiers N, Rives IC, Alisjahbana A, et al. Distinct developmental pathways from blood monocytes generate human lung macrophage diversity. *Immunity* 2021;54:259–75.
53. Kim N, Kim HK, Lee K, Hong Y, Cho JH, Choi JW, et al. Single-cell RNA sequencing demonstrates the molecular and cellular reprogramming of metastatic lung adenocarcinoma. *Nat Commun* 2020;11:2285.
54. Garrido-Martin EM, Mellows TWP, Clarke J, Ganesan A-P, Wood O, Cazaly A, et al. M1(hot) tumor-associated macrophages boost tissue-resident memory T cells infiltration and survival in human lung cancer. *J Immunother Cancer* 2020; 8:e000778.
55. Mao X, Yang X, Chen X, Yu S, Yu S, Zhang B, et al. Single-cell transcriptome analysis revealed the heterogeneity and microenvironment of gastrointestinal stromal tumors. *Cancer Sci* 2021;112:1262–74.
56. Zhang L, Li Z, Skrzypczynska KM, Fang Q, Zhang W, O'Brien SA, et al. Single-cell analyses inform mechanisms of myeloid-targeted therapies in colon cancer. *Cell* 2020;181:442–59.
57. Pan Y, Lu F, Fei Q, Yu X, Xiong P, Yu X, et al. Single-cell RNA sequencing reveals compartmental remodeling of tumor-infiltrating immune cells induced by anti-CD47 targeting in pancreatic cancer. *J Hematol Oncol* 2019;12:124.
58. Chen S, Zhu G, Yang Y, Wang F, Xiao YT, Zhang N, et al. Single-cell analysis reveals transcriptomic remodellings in distinct cell types that contribute to human prostate cancer progression. *Nat Cell Biol* 2021;23:87–98.
59. Uhlen M, Fagerberg L, Hallstrom BM, Lindskog C, Oksvold P, Mardinoglu A, et al. Proteomics. Tissue-based map of the human proteome. *Science* 2015;347: 1260419.
60. DeNardo DG, Ruffell B. Macrophages as regulators of tumour immunity and immunotherapy. *Nat Rev Immunol* 2019;19:369–82.
61. Howard LE, Zhang J, Fishbane N, Hoedt AM, Klaassen Z, Spratt DE, et al. Validation of a genomic classifier for prediction of metastasis and prostate cancer-specific mortality in African-American men following radical prostatectomy in an equal access healthcare setting. *Prostate Cancer Prostatic Dis* 2019; 23:419–28.
62. Comito G, Giannoni E, Segura CP, Barcellos-de-Souza P, Raspollini MR, Baroni G, et al. Cancer-associated fibroblasts and M2-polarized macrophages synergize during prostate carcinoma progression. *Oncogene* 2014;33:2423–31.
63. Erlandsson A, Carlsson J, Lundholm M, Fält A, Andersson S-O, Andrén O, et al. M2 macrophages and regulatory T cells in lethal prostate cancer. *Prostate* 2019; 79:363–9.
64. Hayashi T, Fujita K, Nojima S, Hayashi Y, Nakano K, Ishizuya Y, et al. High-fat diet-induced inflammation accelerates prostate cancer growth via IL6 signaling. *Clin Cancer Res* 2018;24:4309–18.
65. Hodi FS, O'Day SJ, McDermott DF, Weber RW, Sosman JA, Haanen JB, et al. Improved survival with ipilimumab in patients with metastatic melanoma. *N Engl J Med* 2010;363:711–23.
66. Robert C, Thomas L, Bondarenko I, O'Day S, Weber J, Garbe C, et al. Ipilimumab plus dacarbazine for previously untreated metastatic melanoma. *N Engl J Med* 2011;364:2517–26.

67. Reck M, Rodríguez-Abreu D, Robinson AG, Hui R, Csósz T, Fülöp A, et al. Pembrolizumab versus chemotherapy for PD-L1-positive non-small-cell lung cancer. *N Engl J Med* 2016;375:1823–33.
68. Antonia SJ, Villegas A, Daniel D, Vicente D, Murakami S, Hui R, et al. Durvalumab after chemoradiotherapy in stage III non-small-cell lung cancer. *N Engl J Med* 2017;377:1919–29.
69. Ardolino L, Joshua A. Immune checkpoint inhibitors in malignancy. *Aust Prescr* 2019;42:62–67.
70. Bellmunt J, de Wit R, Vaughn DJ, Fradet Y, Lee JL, Fong L, et al. Pembrolizumab as second-line therapy for advanced urothelial carcinoma. *N Engl J Med* 2017; 376:1015–26.
71. Kwon ED, Drake CG, Scher HI, Fizazi K, Bossi A, van den Eertwegh AJM, et al. Ipilimumab versus placebo after radiotherapy in patients with metastatic castration-resistant prostate cancer that had progressed after docetaxel chemotherapy (CA184-043): a multicentre, randomised, double-blind, phase 3 trial. *Lancet Oncol* 2014;15:700–12.
72. Beer TM, Kwon ED, Drake CG, Fizazi K, Logothetis C, Gravis G, et al. Randomized, double-blind, phase III Trial of ipilimumab versus placebo in asymptomatic or minimally symptomatic patients with metastatic chemotherapy-naive castration-resistant prostate cancer. *J Clin Oncol* 2017;35: 40–47.
73. Vitkin N, Nersesian S, Siemens DR, Koti M. The tumor immune contexture of prostate cancer. *Front Immunol* 2019;10:603.
74. Kuniwa Y, Miyahara Y, Wang HY, Peng W, Peng G, Wheeler TM, et al. CD8+ Foxp3+ regulatory T cells mediate immunosuppression in prostate cancer. *Clin Cancer Res* 2007;13:6947–58.
75. Strasner A, Karin M. Immune infiltration and prostate cancer. *Front Oncol* 2015; 5:128.
76. Ebel K, Babaryka G, Frankenberger B, Stief CG, Eisenmenger W, Kirchner T, et al. Prostate cancer lesions are surrounded by FOXP3+, PD-1+ and B7-H1+ lymphocyte clusters. *Eur J Cancer* 2009;45: 1664–72.